Memoirs of the School of Engineering, Okayama University, Vol. 16-2, March 1982

EXAFS Study on Local Structure of Iron Crystal by the Use of Asymmetrical Monochromator and PSPC

M. Hida, H. Maeda, K. Tanabe, N. Kamijo and H. Terauchi

(Received March 5, 1982)

Synopsis

The EXAFS spectroscopy equipment constructed from an asymmetrical cut flat monochromator and PSPC is applied to the structural determination of pure α-iron which has small difference (0.038nm) in the first and second nearest neighbour distance. The efficiency of the curve fitting method for the two shell model of known structure material (α-iron) is discussed, in addition to describing the details of the experimental procedure of our new type of spectrometer and of the EXAFS data analysis.

1. Introduction

The extended X-ray absorption fine structure (EXAFS) spectroscopy is one of the most powerful technique for determing many structural parameters associated with the short range environment surrounding a specific element. The technique has been widely applied to the structural determination of the coordination number and distance of atoms surrounding X-ray absorbing atoms. Recently much attentions have been to study of the compositional fluctuation and local atomic arrangement in solid solution[1, 2, 3] and amorphous alloys [4 to 9], and of the disorder due to thermal and static displacement [10 to 19].

Here we apply the EXAFS spectroscopy equipment constructed from an asymmetrical cut flat monochromator and position sensitive proportional counter (PSPC) to the structural determination of body centered cubic crystal, iron which has small difference (0.038nm) in the first and the second nearest neighbour distance. The peaks corresponding to

the radial structural function obtained from Fourier transform of EXAFS spectrum, $\chi(k)$, were analyzed with a least-squares curve fitting method [20]. Due to the lack of the resolution in real space the first peak contains two shells in case of iron as well as hexagonal crystal, zinc [19]. In this paper we will verify the efficiency of the curve fitting method for the two shell model of known material, in addition to describing the details of the experimental procedure and data analysis.

2. Experimental Procedure

2.1 X-ray Absorption Measurements

The continuous radiation of a 6kW X-ray generator unit with a rotating copper anode (operating at 18kV and 40mA), which has been dispersed by an asymmetrically cut flat crystal monochromator in the magnifying mode silicon (2 2 0) crystal (size, 100 x 30 x 6mm^3, and lattice spacing, d_{220} = 0.191997nm) on a goniometer (250mm in radius).

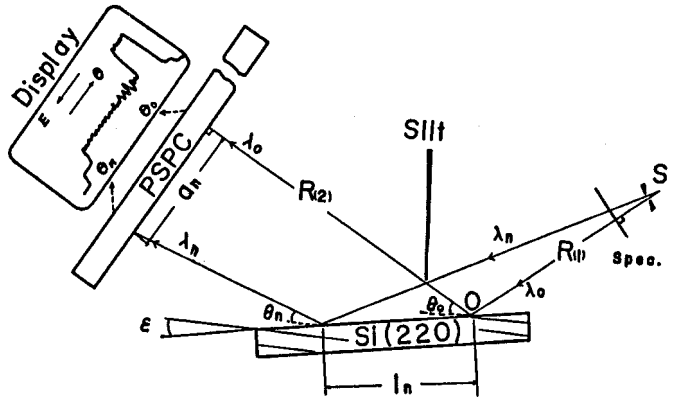

Fig. 1 Schematic diagram of the X-ray spectrometer, ε is the angle between the surface and the reflection plane (2 2 0) of the asymmetrical monochromator, θ the Bragg angle, λ the X-ray wave length, $R_{(1)}$ the distance from X-ray source (S) to the rotation centre (O) of the monochromator, $R_{(2)}$ the perpendicular distance from the center to the position sensitive proportional counter (PSPC).

Fig. 1 shows a schematic diagram of the X-ray spectrometer equipped with a position sensitive proportional counter (PSPC). The PSPC used in our laboratory is 50mm in width. The EXAFS region, up to 1 keV (0.160×10^{-15}J) above absorption edge corresponding to the utmost extent of a few degrees in Bragg angle, is sufficiently covered by the asymmetrically cut flat crystal. The monochromator is available to obtain high resolution in energy. The energy resolution is estimated to be ~4 eV (0.60aJ) from a half value width of Cuk_{α_1}. This PSPC method is better than the ordinal laboratory step scanning method [2, 21] in respect that X-ray source intensity fluctuation over long period of time can be neglected by PSPC method. The principle and the details of this method are as follows.

2.1.1 Detector System and X-ray Source

The system is consisted of PSPC (Ar 90%-CH_4 10% gas flow at 0.3 MP_a), timing single channel analyser, time to amplitude converter, puls hight analyser, high tension and CRT display. The adequate stability of gas flow and electronics units is required to measure the X-ray absorption. Before using the system, it should be stanby for a long time, for example ten days for gas flow and two days for the electronics units at least. Anode target has to be selected so that the EXAFS signal is not disturved by fluorescent emission X-rays of the impurity element in target and target material itself. The tungsten contamination on target decreases the singnal to noise ratio. From this point, Synchrotron Orbital Radiation (SOR) is the best X-ray source for EXAFS.

2.1.2 Optical Alignment and Apparatus Constant

a) As a divergent X-ray beam is used in this method, the channel number, N_0 which the incident beam impinges perpendiculary on PSPC detector at 2θ = 0.000 degree, must be found. In order to perform this object, goniometer setting is refined untill a peak position made by two kinds of slit system (consisted of the 1st, 2nd and 3rd slit, also see Fig. 2) coincides with each other. The peak channel, N_0 is 530.74 and 530.79 for each slit system in present work. The above precise peak channel is calculated from three channels near the center of the real peak by using interpolation of quadratic function.

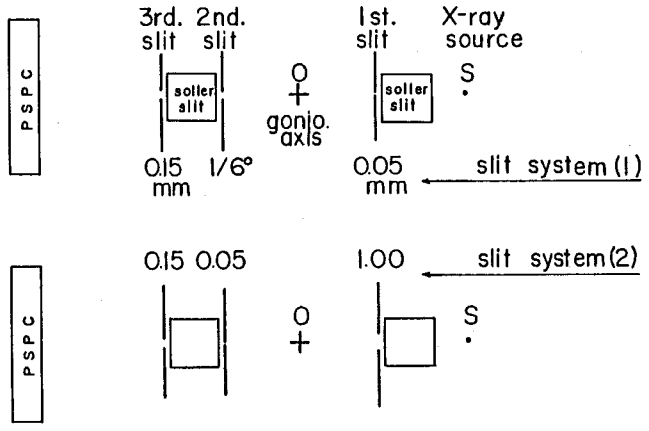

Fig. 2 Two kinds of slit system for the purpose of determing the channel number which the incident beam impinges perpendiculary on PSPC at 2θ = 0.000 degree.

b) Conversion of each channel into energy is made by following formulae,

$$a_n = f\,(n_0 - n_n), \tag{1}$$

$$\sin 2\varepsilon l_n^2 + \{R_{(1)}\sin(\theta_0 + \varepsilon) + R_{(2)}\sin(\theta_0 - \varepsilon) - a_n\cos(\theta_0 - \varepsilon)\}l_n - a_n R_{(1)} = 0, \tag{2}$$

$$\theta_n = \tan^{-1}\{(R_{(1)}\sin\theta_0 + l_n\sin\varepsilon)/(R_{(1)}\cos\theta_0 + l_n\cos\varepsilon)\}, \tag{3}$$

$$E_n = k\nu = 12.39810/2d_{220}\sin\theta_n, \tag{4}$$

where f is the length per channel (mm/ch), d_{220} (0.191997nm) is lattice spacing of reflection plane of the monochromator, and other notations are shown in Fig. 1. The distance $R_{(1)}$, X-ray source to monochromator and $R_{(2)}$, monochromator to PSPC are determicned by using a suitable characteristic spectra (k_{α_1}, k_{α_2} and $k_{\beta_{1,3}}$ etc.) and following expression,

$$R_{(1)}\sin(\theta_0 - \theta_n)\sin(\theta_n + \varepsilon) + R_{(2)}\sin(\theta_0 - \theta_n)\sin(\theta_n - \varepsilon) = a_n\cos(\theta_0 - \theta_n)\sin(\theta_n - \varepsilon). \tag{5}$$

A special ordered cover which has three slits of 0.05mm in width at interval of 20mm in length is inserted into PSPC window as the fourth slit in order to estimate the factor f. Using the first and fourth slit, the peak channel corresponding to the position of each slit of the three slits is searched, and the linear function of length vs channel number is obtained by using a least squares method. The factor, f, is determined to be 0.06294(6)(mm/ch) from the above mentioned procedure.

c) After removing the first slit, the determination of N_0 is performed by fixing the position of PSPC covered with a slit (0.05mm) at the center of PSPC. The average value of the peak channel number, N_0, is 527.78 for $2\theta = 0.000 \pm 0.001^\circ$.

d) After the monochromator of silcon crystal (reflection plane, (2 2 0))is mounted, the axial alignment of the monochromator is performed by using goniometer head and Cuk_{α_1} line ($2\theta = 47.30572^\circ$, $\omega' = \omega - \varepsilon = \omega - 10.570^\circ$, $\omega \equiv \theta$). Fig. 3 shows the profiles of Cuk_{α_1} and Cuk_{α_2} in the case of the best axial alignment.

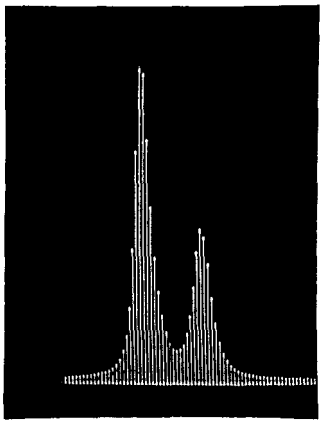

Fig. 3 The profiles of Cuk_{α_1} and Cuk_{α_2} for the best axial alignment is shown on the display. From the profile, the energy resolution is obtained to be ~4.0 eV ($\sim 6.4 \times 10^{-19}$J).

The peak of Cuk_{α_1} stands at 525.78ch, and the energy resolution is ~4.0 eV (6.4×10^{-19}J) above mentioned.

e) We measured the peak channel of Cuk_{α_1}, Cuk_{α_2}, and $Cuk_{\beta_{1,3}}$ by $2\theta - \omega$ scanning to determine the $R_{(1)}$ and $R_{(2)}$, and the following data are obtained:

2θ	ch. no. of k_{α_1}	ch. no. of k_{α_2}	ch. no. of $k_{\beta_{1,3}}$
50.00°	119.93	138.44	———
49.00°	274.61	292.86	———
48.00°	423.67	441.25	———
47.00°	570.50	587.65	———
46.00°	717.97	735.00	———
45.00°	867.43	884.49	———
44.00°	———	———	287.48
43.00°	———	———	449.53
42.00°	———	———	608.65
41.00°	———	———	770.05
40.00°	———	———	930.70

$R_{(1)}$ and $R_{(2)}$ are calculated from the data by the least squares method of the equation (1 to 4). As the results, $R_{(1)}$ and $R_{(2)}$ are 238.00(6) and 483.24(6) mm, respectively.

The final setting of $2\theta_0$ (= 51.60°) is carried out ot cover the EXAFS region (7.03~12.3 keV, $Fek_{abs.\ edge}$ = 7.1162 keV 1 keV = 1.60×10^{-16} J).

f) It is important that the PSPC detector is protected carefully from back-ground intensity caoused by X-ray scattering from air to improve the signal-to-noise ratio of EXAFS. X-ray path is covered by metal in addition to a large half slit (see Fig. 1). Optimum attenuation ud (2.0~2.5) of specimen should be prepared to obtain good signal-to-noise ratio of EXAFS [22, 23]. Accelerating voltage of target should be lowered than twice the threshold energy of k edge to prevent the harmonics of X-ray. In this work, the voltage has been decreased to 16 kV for cold worked iron. Specimen is oscillated to avoid the noise caused by density fluctuation of specimen. This fluctuation is pronounced especially in powder specimen. The contamination of string anode in PSPC affects counting rate of photon.

2.1.3 Preparation of Specimen and Practice of Measurement

The rod shaped (15mmϕ) pure iron (producted by Johnson Mathey Co.) is cold rolled to ~0.1mm in thickness. Some of the iron ribbons are annealed in vacuum for 2hrs at 1170k. The cold worked and annealed iron (here after, abbreviated to an-Fe and cw-Fe, respectively) ribbons are electrolitically polished to foil (~7μm in thickness).

The sequence of the intensity measurement for the absorption of X-ray is IS (an-Fe)→ IO → IS (cw-Fe). Where IS (an-Fe), IO and IS (cw-Fe) are the intensity of transparent X-ray through the anneald iron foil, non specimen and the cold worked iron foil, respectively. The attenuation μd is calculated from the following relation,

$$IS = IO \exp(-\mu d). \qquad (6)$$

In the present work aluminium foil (~45μm) was used in stead of non specimen (IO). Fig. 4 shows the IS (an-Fe), IO (Al) and IS (cw-Fe) versus channel. The irregular intensity profile caused by the contamination of the anode string in PSPC is observed around the 500 channel. The contaminaltion decrease the counting efficiency.

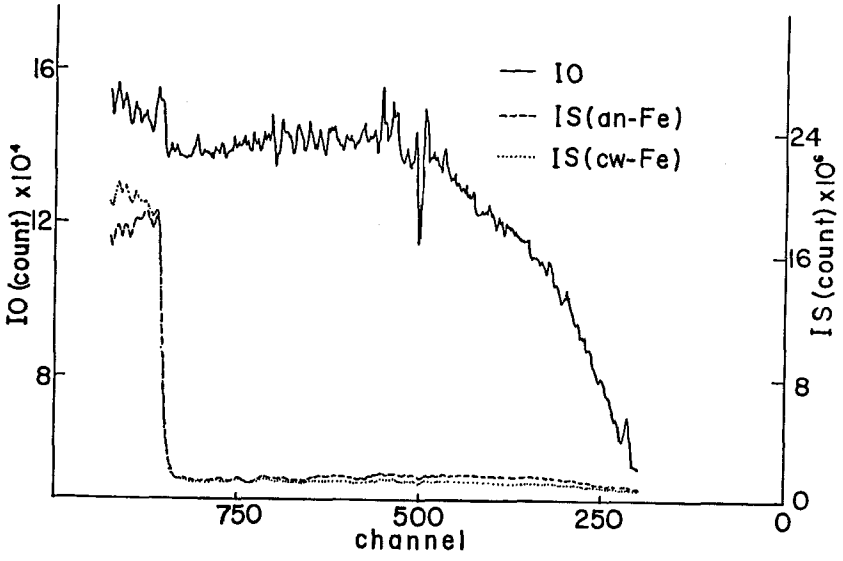

Fig. 4 The intensity profile of X-ray through the specimen of annealed iron (an-Fe), cold worked iron (cw-Fe) and alminium foil vs. channel number.

2.2 EXAFS Data Analysis

Fig. 5 shows typical plots of the attenuation (μd) as a function of X-ray photon energy (E) below and above the k edge of iron, 1.13775 x 10^{-15}J [24] for specimens of an-Fe and cw-Fe. The background ($\mu_v d$) due to excitation of higher shells and second-order reflections has been subtracted from μd by using a Victoreen's fit[25] on the low energy side of the k edge, yielding the k-shell attenuation, $\mu_k(E)d$ (= $\mu d - \mu_v d$) due to the FeK-shell solely. The difference in the slop of the Victoreen's fit between an-Fe and cw-Fe depends upon the accel erating voltage on the target.

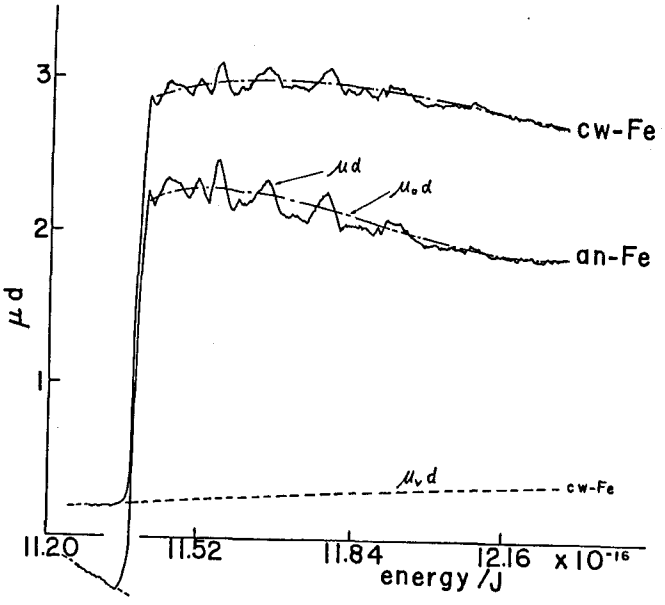

Fig. 5 The X-ray attenuation (μd) near the Fe-K edge of an-Fe and cw-Fe vs. X-ray energy.

For the EXAFS analysis, it is necessary to define the normalized fine structure (also refered to the structure as EXAFS signal),

$$\chi(k) = (\mu_k - \mu_0)/\mu_0 \qquad (7)$$

as a function of the photoelectron wave vector (k), where μ_k and μ_0 are the k-shell absorption coefficients for the atom in its environment and the isolated atom, respectively. The smooth mean value ($\mu_0 d$) was determined by using a cubic spline technique (in the present study,

the region of k is divided into four sections with $\Delta k \approx 30 nm^{-1}$ each). The equation for the EXAFS function, assuming no multiple scattering, is given by

$$\chi(k) = \sum_j (N_j/k_j R_j^2) |f_j(k)| \exp(-2k^2\sigma_j^2) \exp(-2R_j/\lambda_j) \sin[2kR_j + \delta_j(k)], \quad (8)$$

or its abbreviated form,

$$\chi(k) = \Sigma A m_j(k) \sin\phi(k), \quad (9)$$

where k is the wave vector of the ejected photoelectron, N_j the number of atoms in the j-th shell at distance R_j, λ_j the photoelectron mean free path. $f_j(k)$ is the back scattering amplitude of photoelectrons, σ_j^2 the mean-square atomic displacement arising from both static and thermal disorder, $\delta_j(k)$ the phase shift containing contributions from both atoms of absorbing photon and scattering photoelectron at the j-th shell. This quantity can be extracted from the EXAFS signal by a variety of methods [21, 26, 27].

As the first step in the analysis, $\chi(k)$ has been multiplied by the factor k^n, and then is Fourier transformed as follows

$$\psi(R) = \frac{1}{\sqrt{\pi}} \int_{k_{min}}^{k_{max}} k^n \chi(k) w(k) \exp(-2\pi kR) dk, \quad (10)$$

where

$$w(k) = \frac{1}{2} \{1 - \cos 2\pi [(k - k_{min})/(k_{max} - k_{min})]\}.$$

Hanning's window function, w(k) is used in order to avoid data truncation effects in the regions of k values corresponding to the first and last 10% of the range investigated [28]. The power (n) is 1 to 3, which is selected to obtain the best peak separation in R-space. For the purpose of curve fitting, the high frequency noise and residual background in each spectrum are further removed by a Fourier filtering technique. It involves selecting the distance (R) range to be kept, and backtransforming to k-space, in addition to Fourier transforming the $k^n\chi(k)$ into R-space. Hanning's window function is also employed to filter a certain band of the radial structural function (RSF).

The resulting filtered data are applied to the following curve fitting method. Carrying out the non-linear least-squares program of

Marqiard't [20] method, the Fourier filtered data are fitted with the function (8) or (9), in which $f_j(k)$ and $\delta_j(k)$ are parameterized as follows [26]:

$$f_j(k) = A_j/\{1 + B_j^2(k - C_j)^2\},$$
$$\delta_j(k) = a_j + b_jk + c_jk^2 + d_j/k^3, \qquad (11)$$
$$k = \sqrt{k'^2 - 2(\Delta E_{0j})/7.62},$$

where k' and ΔE_0(eV) are the experimental wave vector and the difference in energy threshold between theory and experiment, respectively. The amplitude parameter $\{A_j, B_j, C_j\}$ and phase shift parameter $\{a_j, b_j, c_j, d_j\}$ used for the interesting sample are determined from the refinement. The least-squares refinement is applied to obtain the structural parameter, $\{N_j, R_j, \sigma_j, \lambda_j, \Delta E_{0j}\}$, of unknown material.

3. Results and Discussion

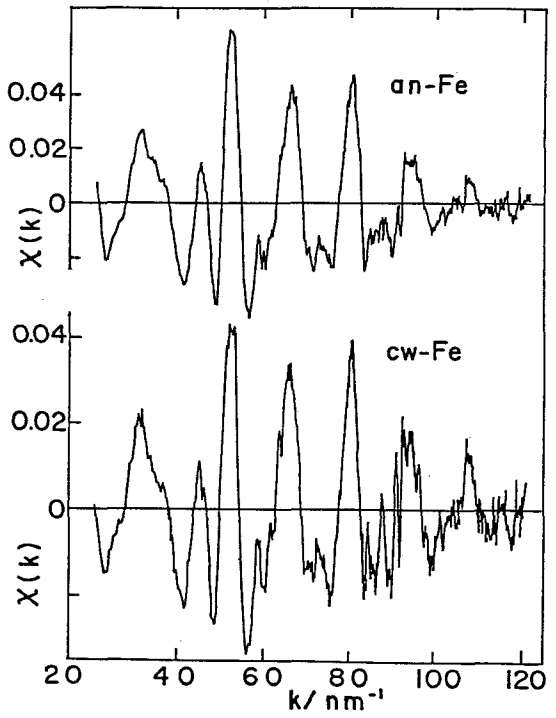

Fig. 6 The normalized EXAFS spectra for an-Fe and cw-Fe.

Fig. 6 shows the EXAFS signal (or spectrum) of annealed and cold worked iron. The Fourier transform of these spectra (k = 30 to 150nm^{-1}) multiplied by k^3 provides the radial distribution function shown in Fig. 7. This radial structural function (RSF) is in good agreement with the other study [29, 30]. The shell radii of the first ot fifth are in the three peaks (I toIII) in Fig. 7. The first peak in the absolute value of $\psi(R)$ contains the first and second nearest neighbour shells, not being separated each other such as an example of copper sample [18, 31]. The imaginal part of $\psi(R)$ in Fig. 7 shows the position of the first and second shell, (Ia, Ib) 0.2068 and 0.2445nm, respectively. The difference of the position is 0.0377nm corresponding to that of the first and second neighbour distance (0.0384nm) obtained from X-ray diffraction method.

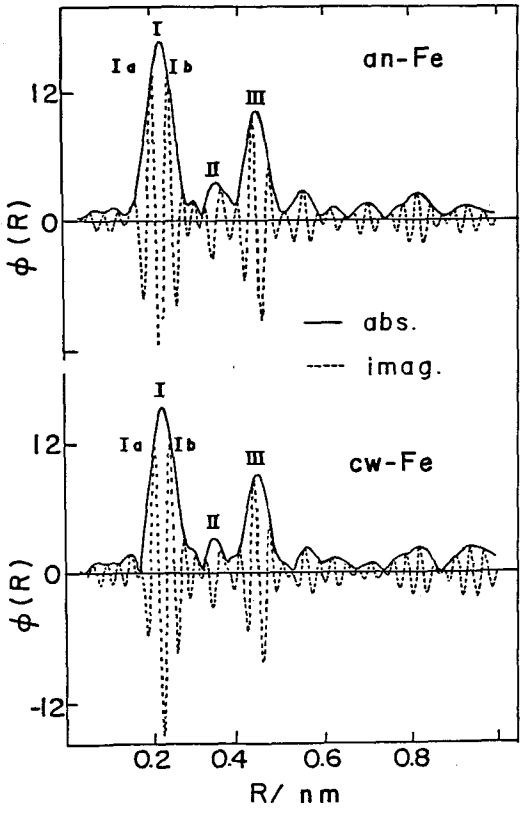

Fig. 7 Magnitude (solid line) and imaginal (dashed line) of Fourier transform of $k^3\chi(k)$ for annealed and cold worked iron. These transforms are taken over the k-space range 30 to 150^{-1}nm with k = 0 being chosen at 7.1162 keV (1.13775 x 10^{-15}J).

The first peak of annealed iron in the Fourier transform function $\{\psi_1(R) + \psi_2(R)\}$ is filtered with a narrow band of width ranging from one-side to the other-side hollow of the peak, and transformed back to k-space, $k^3\{\chi_1(k) + \chi_2(k)\}$. The parameters, {A, B, C, a, b, c, d, ΔE} in the amplitude and phase-shift function (11) are determined by curve fitting with the resultant EXAFS, $k^3\{\chi_1(k) + \chi_2(k)\}$ of annealed iron under following condition,

$N_1 = 8.00$, $R_1 = 0.2482$nm .....<111> direction,
$N_2 = 6.00$, $R_2 = 0.2866$nm .....<100> direction,
$\{\sigma_1 \neq \sigma_2, \lambda_1 = \lambda_2\}$,

and in the case of that the "transferability" is satisfied [27, 32],

$$\{A_1, B_1, C_1, a_1, b_1, c_1, d_1, \Delta E\} = \{A_2, B_2, C_2, a_2, b_2, c_2, d_2, \Delta E\}$$

in equation (11). The other condition of $\sigma_1 = \sigma_2$ may be unreasonable, because the Young's modulus is anisotropic ($E_{<111>} > E_{<100>}$, [33]) and the expected relation must be σ_1 ($=\sigma_{<111>}$) < σ_2 ($= \sigma_{<100>}$). Therefore, the reasonable condition on determing the amplitude and phase parameters is $\sigma_1 \neq \sigma_1$ and $\lambda_1 = \lambda_2$. The sequence of curve fitting is as follows,

step (1) $\{A, B, C, \sigma_1, \sigma_2, \lambda\}_{(1)}$ in the amplitude of $\{\chi_1(k) + \chi_2(k)$ is floated, and as the initial value of these parameters[26], {0.679, 0.1939, 6.355, 0.005nm, 0.005nm, 0.500nm} is adopted.

step (2) $\{a, b, c, d, \Delta E\}_{(2)}$ in $\{\chi_1(k) + \chi_2(k)\}$ is floated and {A, B, C, σ_1, σ_2, λ} is fixed to be $\{A, B, C, \sigma_1, \sigma_2, \lambda\}_{(1)}$

step (3) $\{A, B, C, \sigma_1, \sigma_2, \lambda\}_{(3)}$ in $\{\chi_1(k) + \chi_2(k)\}$ is floated and $\{a, b, c, d, \Delta E\}$ is fixed to be $\{a, b, c, d, \Delta E\}_{(2)}$

step (4) $\{A, B, C, \sigma_1, \sigma_2, \lambda, a, b, c, d, \Delta E\}$ in $\{\chi_1(k) + \chi_2(k)\}$ is floated.

These parameters obtained through above sequence are listed in Table 1. For the condition of $\lambda_1 = \lambda_2 \neq$ constant, λ does not converge. As far as the "transfarbility" is introduced, σ_1 become larger than σ_2. The parameters $\{A_1, B_1, C_1, a_1, b_1, c_1, d_1\}$ have been also obtained from Fe-Fe pair in metalic ocmpound, Fe_2Zr[5] and from the theoretical evaluation [26] (see two lines from bottom in Table 1). The present data are somewhat similar to the theoretical values.

Table 1

The parameters of an-Fe, obtained by curve fitting method[26]

Condition		shell	parameters of amplitude term					
			N	A	B	C	σ(nm)	λ(nm)
	$\lambda_1=\lambda_2$	1	(8.00)	0.55(5)	0.26(2)	6.57(10)	0.0073(7)	(0.500)
$\sigma_1=\sigma_2$	=0.500	2	(6.00)				0.0038(13)	(0.500)
Fe_2Zr [5]		1	(6.00)	2.45988( )	0.23134( )	14.32337( )	———	———
Reference[26]		1	(8.00)	0.679	0.1939	6.355	———	———

Condition		shell	parameters of phase term					
			R(nm)	a	b	c	d	ΔE(keV)
	$\lambda_1=\lambda_2$	1	(0.2482)	7.69(2)	-1.16(3)	0.018(2)	-110.1(18)	-0.026
$\sigma_1=\sigma_2$	=0.500	2	(0.2866)					
Fe_2Zr [5]		1	(0.250)	-12.6648( )	-0.90938( )	0.01209( )	8.4406( )	
Reference[26]		1	(0.2482)	8.452	-1.1931	0.02522	-47.35	

( ) : fixed value

The most reasonable parameters in the present study (see Fig. 8, the parameters on the third line from bottom of Table 1 illustrate the degree of the fitting as shown in Fig. 8) are able to apply to the determination of the structure parameters of cold worked iron $\{N_1, R_1, \sigma_1, N_2, R_2, \sigma_2, \Delta E\}$. The results obtained are listed in Table 2. R_1 and R_2 are increased and N_1 and N_2 are decreased by heavy cold working. The relation, $\sigma_1 > \sigma_2$ is also conserved in cold worked iron. The parameter curve fitting for annealed iron will be carried out under the condition of non-transferability, $\{A_1, B_1, C_1, a_1, b_1, c_1, d_1\} \neq \{A_2, B_2, C_2, a_2, b_2, c_2, d_2\}$.

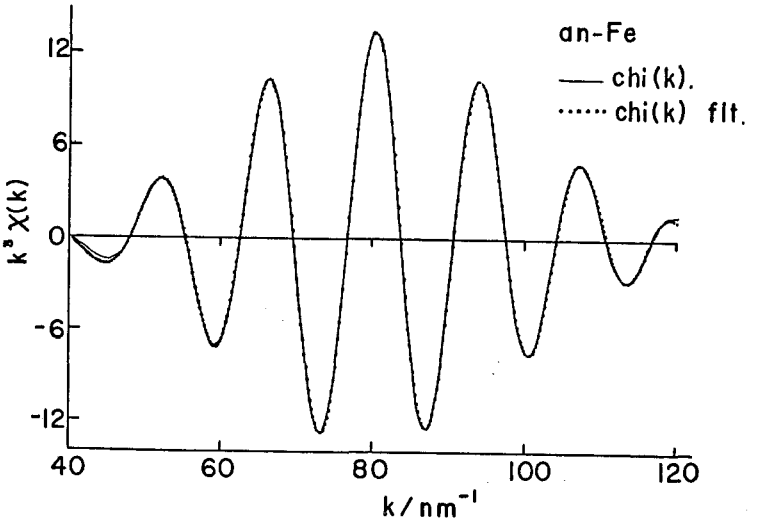

Fig. 8 The solid curve shows the measured value of the inverse Fourier transform for the first peak (0.152 to 0.285nm) of an-Fe. The dotted line shows the best fit to the measured value with the parameter (see Table 1) in the case of amplitude and phase transferability conserved.

Table 2

Structural parameter of cw-Fe

Shell No.	N	R(nm)	σ(nm)	λ(nm)
1	6.26(73)	0.2522(5)	0.00562(66)	(5.00)
2	3.55(67)	0.2880(5)	0.00199(301)	(5.00)

References

[1] A.Fontain, P.Lagarde, A.Naudon, D.Raoux and D.Spanjaard, Phil.Mag. B40, 17 (1979).
[2] H.Maeda, T.Tanimoto, H.Terauchi and M.Hida, phys.stat.sol. (a)58, 629 (1980).
[3] J.Mimault, A.Fontaine, P.Lagarde, D.Raoux, A.Sadoc and D.Spanjaard, J.Phys.F : Metal Phys. 11, 1311 (1981).
[4] S.E.Sayer, Pro VII.Internat.Conf. Amorphous and Liquid Semiconductors, Edinbrough 1977 (P.61).
[5] H.Maeda, H.Terauchi, N.Kamijo, M.Hida and K.Osamura, Pro.VI.Internat. Conf. on Rapidely Quenched Metals, Sendai 1981 (to be published).
[6] P.H.Fuoss and P.Eisenberger, W.K.Warburton and A.Bienenstock, Phys.Rev.Letters 46, 1537 (1981).
[7] H.Terauchi, H.Maeda, K.Tanabe, N.Kamijo, M.Hida, M.Takashige, T.Nakamura, H.Ozawa and R.Uno, J.Phys.Soc. of Japan 50, 3977 (1981).
[8] H.Maeda, N.Kamijo, H.Terauchi, M.Hida and H.Kawamura, J.Phys.Soc. of Japan, to be submitted.
[9] F.Evangelisti and M.G.Proietti, A.Balzarotti, F.Comin, L,Incoccia and S.Mobilo, Solid State Commun. 37, 413 (1981).
M.De Crescenzi, A.Balzarotti, F.Comin, L.Incoccia, S.Mobilio and N.Matta, ibid 37, 921 (1981).
[10] G.Beni and P.M.Platzman, Phys.Rev. B14, 1514 (1976).
[11] S.J.Gurman and J.B.Pendry, Solid State Commun. 20, 287 (1976).
[12] P.Rabe, G.Tolkiehn and A.Werner, J.Phys.C : Solid State Phys. 12, L545 (1979).
[13] R.B.Greegor and F.W.Lytle, Phys.Rev. B20, 4902 (1979).
[14] P.Eisenberger and G.S.Brown, Solid State Commun. 29, 481 (1979).
[15] P.P.Lottici and J.J.Rehr, Solid State Commun. 35, 565 (1980).
[16] C.G.Olson and D.W.Lynch, Solid State Commun. 36, 513 (1980).
[17] P.Eisenberger and B.Lengeler, Phys.Rev. B22, 3551 (1980).
[18] M.Hida, H.Maeda, N.Kamijo and H.Terauchi, Phys.Stat.Sol. (a)66, NO. 1 (1982).
[19] E.D.Crozier and A.J.Seary, Can.J.Phys. 58, 1388 (1980).
[20] D.W.Marquardt, J.Soc.Indust. Appl.Math. 11, 443 (1963).
[21] F.W.Lytle, D.E.Sayers and E.A.Stern, Phys.Rev. B11, 4825 (1975).
[22] B.M.Kincaid, SSRP Tech.Rep. No. 75, 3 (1975).
[23] E.A.Stern and K.Kim, Phys.Rev. B23, 3781 (1981).
[24] International Tables for X-Ray Crystallography, Vol. IV, section 1.1, Kynoch Press, Birmmgham 1974.

[25] ibid, vol. III, Section 3.2, Kynoch Press, Birmingham 1968.
[26] B.K.Teo, P.A.Lee, A.L.Simon, P.Eesinberger and B.M.Kincaid, J.Amer, Chem.Soc. 99, 3854, 3856 (1977).
[27] E.A.Stern, D.E.Sayers and F.W.Lytle, Phys.Rev. B11, 4836 (1975).
[28] C.Bingham, M.Godfrey and J.Tukey, IEEE Trans.Audio Electroacoustic AU-15, 56 (1967).
[29] J.Wong, in "Metallic Glasses" ed. by H.J.Güntherodt and H.Beck, Topics in Applied Physics Vol. 46, Springer Verlag, Berlin (1980)
[30] T.Kitano, F.Itoh, T.Kamiyama and K.Suzuki, Fall Meeting (Kyoto, 1981) of Japan Inst. of Met. Proceedings, P.231.
[31] G.Marten, P.Rabe, N.Schwentner and A.Werner, Phys.Rev. B17, 1481 (1978).
[32] P.H.Citrin, P.Eisenberger and B.M.Kincaid, Phys.Rev.Lett. 36, 1346 (1976).
[33] M.E.Fine, Am.Soc.Testing Mat.Bull. 181, 20 (1952).